Role of mTOR Inhibitors in Growth Hormone-Producing Pituitary Adenomas Harboring Different FGFR4 Genotypes

Shahrzad Jalali,* Eric Monsalves,* Toru Tateno, and Gelareh Zadeh

McFeeters-Hamilton Center for Neuro-Oncology Research (S.J., E.M., G.Z.), Princess Margaret Cancer Center (S.J., E.M., T.T., G.Z.), and Division of Neurosurgery (G.Z.), Toronto Western Hospital, Toronto, Canada M5T 2S8

Pituitary adenomas (PAs) are common intracranial lesions. Available medical therapies are limited in PAs, and therefore, it is essential to identify treatments that control PA growth when surgery is not an option. Fibroblast growth factor 4 is implicated in PA pathogenesis; therefore, in this study, we used an isogenic mammosomatotroph cell line (GH4C1) harboring different fibroblast growth factor receptor (FGFR)-4 genotypes to establish and characterize intracranial xenograft mouse models that can be used for preclinical drug testing. We show that proliferating GH4C1 tumors have an average latency of 3 weeks to form. Histological analysis revealed that prototypic FGFR4 (G388) tumors express increased prolactin and less GH, whereas tumors possessing the polymorphic variant of FGFR4 (R388) express increased GH relative to prolactin. All tumors show abundant mammalian target of rapamycin (mTOR) signaling as confirmed using phosphorylated (p)-S6 and p-4E-binding protein 1 as downstream regulators of this pathway. We subsequently demonstrate that the mTOR inhibitor RAD001 decreases tumor growth rate and reduces p-S6 but not p-4E-binding protein 1 activation, regardless of FGFR4 status. More importantly, GH activity was significantly reduced after mTOR inhibition in the R388 polymorphic variant tumors. This reduction was also associated with a concomitant reduction in serum IGF-1 levels in the R388 group. In summary, we demonstrate that the GH4C1 FGFR polymorphic xenograft is a useful model for examining PAs. Furthermore, we show that RAD001 can efficiently reduce tumor growth rate by a reduction in mTOR signaling and more importantly results in control of GH expression and IGF-1 secretion, providing further support for using mTOR inhibitors in PA patients, in particular GH-producing adenomas. **(*Endocrinology* 157: 3577–3587, 2016)**

Pituitary adenomas (PAs) are benign intracranial neoplasms that are prevalent in up to 20% of the general population (1). There are many histological subtypes of PAs, and they can be either hormonally active or inactive presenting with various endocrine abnormalities and clinical manifestations (2). Despite their benign and often indolent nature, PAs have a tendency for invasion into areas surrounding the pituitary fossa such as the optic chiasm and/or into the cavernous sinus (3). Furthermore, most PAs that come to clinical attention are hormonally inactive macroadenomas, typically of gonadotroph differentiation (2), and so do not respond to current medications such as dopamine agonists or somatostatin analogs. The primary therapeutic strategy for most PAs is surgery; however, PA recurrence after surgical resection occurs in approximately 15%–20% of cases (4). Moreover, for those PAs involving surrounding structures, achieving complete resection remains challenging, and therefore, identifying medical therapies that effectively restrict tumor growth is a clinical priority.

ISSN Print 0013-7227 ISSN Online 1945-7170
Printed in USA

Received January 14, 2016. Accepted May 31, 2016.
First Published Online June 7, 2016

For News & Views see page 3400

* S.J. and E.M. contributed equally to this work.

Abbreviations: 4EBP1, 4E-binding protein 1; FGFR, fibroblast growth factor receptor; IHC, immunohistochemistry; MRI, magnetic resonance imaging; mTOR, mammalian target of rapamycin; NOD-SCID, nonobese severe combined immunodeficiency; p, phosphorylated; PA, pituitary adenoma; PC, empty vector; PRL, prolactin; ptd-FGFR, pituitary tumor-derived variant of FGFR; RARE, rapid acquisition relaxation enhancement; SNP, single-nucleotide polymorphism; STAT, signal transducer and activator of transcription; TE, echo time; TR, repetition time; TVDT, tumor volume doubling time.

The molecular mechanisms that are involved in PA initiation and progression are not yet well established. Some molecular initiators of pituitary tumorigenesis have been identified. For example, somatic mutations resulting in G protein abnormalities and subsequent increases in cAMP levels have been identified in a subset of GH-PA (5). RAS mutations also occur, but these are limited to the rare metastatic pituitary carcinoma (6). Further exploration is required to make targeted therapeutics for the management of PAs a realistic option. There has been accumulating evidence to support that modulation of growth factors and their receptors are necessary for normal pituitary growth and function. For example, deletion of fibroblast growth factor-10 or its receptor, the fibroblast growth factor receptor (FGFR)-2IIIb isoform, leads to the failure of pituitary development (7). Dysregulation of these factors may lead to abnormal pituitary growth and tumor development. For example, fibroblast growth factor-2 mRNA has been shown to be overexpressed in PAs (8). Recent interest has focused on FGFR4, which is a 110-kDa transmembrane kinase that is involved in mitogenesis and angiogenesis (9). A 60-kDa N-terminally truncated pituitary tumor-derived variant of FGFR4 (ptd-FGFR4) has been identified in 40%–50% of PAs but not in normal pituitary (10). Preclinical evidence suggests that ptd-FGFR4 but not full-length FGFR4 confers oncogenic properties to pituitary tumor cells. In human PA tissue, positivity for ptd-FGFR4 has been associated with increased PA aggressiveness (11).

Germline allelic alterations in FGFR4 have also been identified in PAs. An adenine to guanine single-nucleotide polymorphism (SNP) at codon 388 of the *FGFR4* gene results in a glycine to arginine substitution in the transmembrane domain of the FGFR4 protein (FGFR4-G388R) (12). This SNP correlates with the increased growth and GH production in GH4C1 cells and human GH-PA tissue. Furthermore, in a knock-in mouse model harboring the FGFR4 SNP, a GH-secreting tumor develops in approximately 12 months (13).

There is a paucity of data regarding downstream molecular mechanisms from FGFR4 in PAs. Ezzat et al (14) have reported that ptd-FGFR4 promotes oncogenic transformation by disturbing the neural cell adhesion molecule-β-catenin complex, thereby disrupting normal cell-to-cell interactions. In their study, an FGFR4 inhibitor was used to restore the neural cell adhesion molecule complex and reduce cell and tumor growth. In the FGFR4-G388R SNP, src and signal transducer and activator of transcription (STAT)-3 serine phosphorylation was shown to promote growth, whereas STAT3 tyrosine phosphorylation modulated hormone secretion (13, 15).

Recent interest has focused on the phosphatidylinositol 3-kinase/mammalian target of rapamycin (mTOR) pathway, the signaling cascade important for maintaining growth and homeostasis within the cell. It is ubiquitously overexpressed in cancer and has been shown to be overexpressed in PAs, particularly in nonfunctioning pituitary adenoma and GH-PA (16, 17). It has been demonstrated that the mTOR inhibitors are effective in PA cells by reducing cell viability and proliferation and also arresting cells early in the cell cycle (18, 19). The phosphatidylinositol 3-kinase/mTOR pathway is frequently initiated by activation of receptor tyrosine kinases that may include FGFR4. The aim of this study is to determine the expression and activation status of the mTOR pathway in different FGFR genotypes (wild type G388 and polymorphic R388) using xenograft mouse model tumors and, furthermore, establish how FGFR variants may influence sensitivity to mTOR inhibition and ultimately hormone levels and tumor growth using RAD001.

Materials and Methods

Cell lines and culture conditions

Rat pituitary GH4C1 mammosomatotroph cells were used for this study. The cell lines were maintained as described previously by (13).

In brief, cells were cultured in Ham's F10 medium, 12.5% horse serum, and 2.5% fetal bovine serum (FBS; Sigma), 2 mM glutamine, 100 IU/mL penicillin, and 100 μg/mL streptomycin (37°C, 95% humidity, 5% $C0_2$ atmosphere incubation).

Plasmids and generation of stable cell lines

Plasmids encoding human prototypic FGFR4 (G388) or the polymorphic form FGFR4 (R388) were generated and stably transfected into GH4C1 as previously described (13). Construct fidelity was confirmed by DNA sequencing after introduction into pcDNA 3.1. Cells were transfected using Lipofectamine 2000 (Life Technologies) according to the manufacturer's instructions. Stable clones were selected using neomycin (G418) at a concentration of 0.7 μg/mL.

Animal models

All animal experiments and protocols were approved by the University Health Network (UHN) Animal Care and Use Committee. Immune-compromised, nonobese severe combined immunodeficiency (NOD-SCID) male mice were purchased from Jackson Laboratory and used for intracranial studies. Cell lines used were GH4C1 cells (parental control), G388, and R388 representing the SNP variant FGRF4-expressing cells. GH4C1 empty vector (PC) transfected cells were also used as controls.

Xenografts were generated as previously described (20). Briefly, 6-week-old NOD-SCID mice were anesthetized and the scalp was opened with a 1-cm incision, and the landmark was identified for injections. Cell lines were stereotactically injected

into the right frontal lobe at 1 mm anterior and 2 mm lateral to bregma at 3 mm depth from the dura. At first, we used a serial dilution of 10^5 and 10^6 cells injected intracranially to optimize the best preclinical models for PA xenografts. Injection of 10^6 cells resulted in very rapid tumor development, precluding accurate growth rate studies on magnetic resonance imaging (MRI). Injection of 10^5 cells resulted in tumors with very long growth latency periods on the order of several months. We therefore chose an intermediate cell number of 500,000 cells that would produce a model that allowed for accurate preclinical studies to examine growth response to therapeutics drug studies. We also confirmed that on immunohistochemical characterization, the tumors we created in this manner maintained hormonal expression pattern, coexpressing GH and prolactin (PRL) in PC, G388, and R388 mice. The R388 tumor expressed more GH relative to the G388 and PC tumors, which was in line with what has been reported previously using these cells (13). All mice were injected on the same day. Mice were monitored closely by serial MRI, starting at week 2 and killed at a fixed time point for all mice at the end of the treatment period to allow a direct comparison and response to treatment between all arms.

To characterize the tumor growth rate using PC, G388, or R388 cell lines, we initially generated xenografts on 30 mice, which included 10 mice in each arm. For drug treatment studies, we generated additional xenografts and each treatment arm included 10 mice. In instances when signs of illness developed, typically characterized by hunched or abnormal posture, decreased movement, lethargy, paralysis, or weight loss prior to end of the treatment period, the mice were killed. Therefore, the final statistical analysis was performed on eight mice in each arm, for which MRI images were available at all time points.

Magnetic resonance imaging

MRI was performed with a 7 Tesla Biospec 70/30 (Bruker Corp), using the B-GA12 gRTient coil insert and 7.2-cm inner diameter linearly polarized volume resonator coil for radiofrequency transmission as detailed previously (21).

The protocol provided a stack of transverse two-dimensional slices with shared geometric prescription (16 × 16 mm field of view), testing multiple contrast mechanisms, as follows: 1) T_2-weighted rapid acquisition relaxation enhancement (RARE) anatomical imaging (echo time [TE] or TE = 72 milliseconds; repetition time [TR] or TR = 5000 milliseconds; RARE factor = 16; readout bandwidth = 50 kHz; 25 × 125 × 500 μm voxels) for 1 minute 20 seconds; and 2) contrast-enhanced, T_1-weighted RARE (TE = 8 msec; TR = 1200 msec; RARE factor = 4; readout bandwidth = 81.5 kHz; 125 × 125 × 500 μm voxels; start imaging at 5 min after contrast) for 1 minute 20 seconds.

For anatomical images, the MRI sequence of T_1 + gadolinium was used and correlated with T_2-weighted images. We found a close correlation between T_1 + gadolinium and T_2 weighted for determining tumor boundaries and overall volume. Therefore, T_2-weighted images were primarily used for calculating longitudinal tumor volume and growth rate in this study (please see detailed below).

Treatment schedule

After an intracranial injection, the tumor development was monitored using MRI, beginning at 2 weeks after the intracranial tumor cell implantation. After tumor formation was noted on MRI, to ensure approximately similar tumor volumes at the start of treatment, mice were randomly stratified into control or treatment arms. Treatment consisted of daily ip injections of 5 mg/kg RAD001 (Cedarlane) or vehicle used as control. Treatment lasted for 3 weeks at which point the mice were killed and their brains extracted and placed into formalin for histological analysis. For five mice in each of the three cell subtypes, tumors were isolated using a surgical microscope and preserved in liquid nitrogen for Western blot analysis (see below for details). MRI was performed weekly on all animals while on treatment to allow tumor volume analysis as detailed below.

Tumor size measurement

Serial magnetic resonance images were used to establish the tumor volumes and growth rates. ITK-SNAP was used to analyze the MR images (www.itksnap.org; [22]). The tumor region of interest on T_2-weighted images was manually defined and used to measure the tumor volume. To estimate the tumor growth rate, we used a previously established formula for measuring a tumor volume doubling time (TVDT): $TVDT = t * \log_2 2/\log 2 (V_f/V_0)$, where t is the time interval between the first and second MRI examinations, V_0 is the initial tumor volume, and V_f is the final tumor volume (23). The TVDT formula has been used by our group to measure tumor growth rate in a previous publication (4, 24). These studies were done by two independent examiners (E.M.) and (S.J.), and there was good interobserver correlation (α = .92).

Immunohistochemistry

Immunostaining was conducted on formalin-fixed, paraffin-embedded lesional tissue in brain sections of control and treated animals. The sections were deparaffinized in xylene and rehydrated in graded ethanol and rinsed in distilled H_2O. After heat-induced antigen retrieval, slides were incubated with primary antibodies with appropriate conditions. Detection was performed using Vectastain ABC reagent and diaminobenzidine chromagen (Vector Labs). Slides were counterstained in Meyer's hematoxylin for 5 minutes, dehydrated with ethanol (70%, 95%, 100%), and mounted. Primary antibodies were MIB-5/Ki-67 (Dako), phosphorylated (p)-S6 (Cell Signaling), p-4E-binding protein 1 (p-4EBP1; Cell Signaling), GH, and prolactin antibodies (kindly provided by the laboratory of Dr Sheeren Ezzat, Princess Margaret Cancer Centre, University of Toronto). All slides were scanned using Zeiss Mirax scanner and analyzed using Mirax Viewer software.

Western blot analysis

To quantify protein expression and phosphorylation in tumor tissue, brains were extracted and tumors immediately isolated and placed in liquid nitrogen for snap freezing. Lysis buffer (0.5% sodium deoxycholate, 0.1% sodium dodecyl sulfate, 1% Nonidet P-40, and 1× PBS) containing proteinase and phosphatase inhibitors was added to tumors, which were then homogenized using a mechanical tissue homogenizer. Total cell lysates were incubated on ice for 30 minutes followed by microcentrifugation at 10 000 × *g* for 10 minutes at 4°C, and the supernatants were collected. Protein concentration was determined by a bicinchonic assay as per the manufacturer's specifications (Pierce Chemicals Co). A total of 40 μg was separated on a 10% SDS-

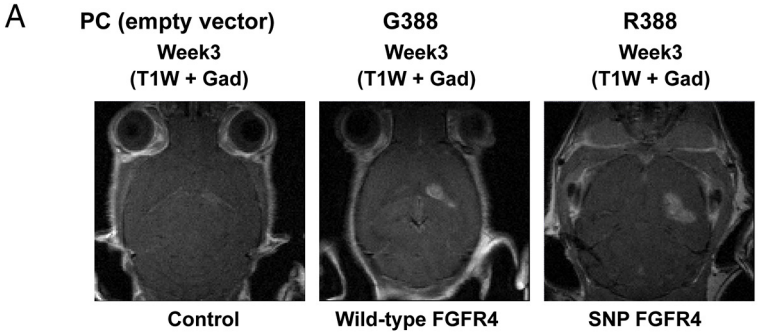

B

Growth Rate

Cell Line	TVDT
PC	12.4 days*
G388	6.7 days
R388	4.8 days

*p<0.05

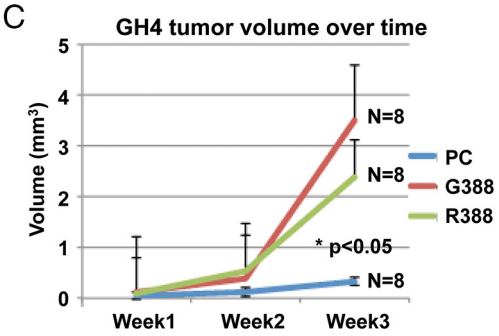

Figure 1. MRI and volumetric analysis for three different GH4C1 cell groups (PC, G388, andR388). A, T1-weighted + gadolinium MRI scans of axial plane demonstrating tumor development 3 weeks after intracranial injection of 5 ∗ 105 GH4C1 cell lines. B, Volumetric data from the intracranial GH4C1 tumors (PC, G388, or R388) were incorporated into the formula for estimating TVDT, and a growth rate was generated (in days). PC had a significantly longer TVDT (slower growth rate) than G388 or R388 tumors. *, $P < .05$ (n = 8 in each group [PC, G388, R388]).

PAGE and blotted onto nitrocellulose membranes (Bio-Rad Laboratories) using a semidry turbo transfer apparatus (Bio-Rad Laboratories). After blocking the membrane with PBS (or TBS) containing 5% nonfat dry milk and 0.05% Tween 20 (Sigma-Aldrich) for 1 hour, the membranes were incubated with primary antibodies overnight at 4°C. The following antibodies were used: 1:1000 p-4EBP1 (Cell Signaling); 1:2000 p-S6 (Cell Signaling); 1:1000 GH (laboratory of Dr Sheeren Ezzat, Princess Margaret Cancer Centre, University of Toronto); 1:1000 PRL (laboratory of Dr Sheeren Ezzat, Princess Margaret Cancer Centre, University of Toronto); and 1:500 ki-67 (Dako). Membranes were washed and later incubated with IRDye secondary antibodies against the species, and the primary antibody was derived (Bio-Rad Laboratories). Protein bands were detected using and quantified using LI-COR software.

Enzyme-linked immunosorbent assay

To measure the serum levels of IGF-1, we used an ELISA kit. Mouse whole blood was extracted from the right ventricle of the heart at time the animals were killed, placed in Microvette CB 300z serum extraction tubes, and immediately centrifuged for 5 minutes at 5000 rpm at 4°C. Serum was extracted and stored at −80C. An ELISA was used to measure serum IGF-1 (Quantikine) levels according to the manufacturer's protocol.

Statistical analysis

Nonparametric tests (Kruskall-Wallis, Mann-Whitney *U*) were used to examine the median differences in the tumor growth rates and IGF-1 levels. H-Scoring was used to semiquantify immunohistochemistry (IHC) data. Intensity of the Western blot protein bands was quantified using LI-COR software.

Results

Intracranial GH4C1 tumors harboring either prototypic FGFR4 (G388) or polymorphic FGFR4 (R388) exhibit faster tumor growth rate compared with parental control (PC) tumors

To investigate whether GH4C1 cells give rise to a tumor in the intracranial location, we implanted GH4C1 cells in NOD-SCID mouse brain and followed tumor formation and growth rate as measured by TVDT using MRI analysis. MRI scans showed tumor formation 3 weeks after the intracranial injection of all three different GH4C1 cell lines: PC, G388, and R388 (Figure 1A). To investigate whether the growth rate of the tumors differ between different cell groups, we performed a longitudinal MRI analysis on these mice. Based on our data, the PC tumors exhibited an overall slower growth rate (increased TVDT) relative to the G388 or R388 tumors, which both displayed similar growth patterns (12.4 d vs 6.7 or 4.8 d) ($P = .034$) (Figure 1, A and 1B). Furthermore, we performed IHC for Ki-67, a marker of cell proliferation (Figure 2A). Our data show significantly increased Ki-67 staining in G388 and R388 tumors compared with the PC control tumors ($P < .001$) (Figure 2B), confirming our tumor growth rate analysis data using MRI (Figure 1) in which the PC tumors show the slowest growth rate compared with G388 and R388 tumors.

GH and PRL show differential expression pattern in the GH4C1 intracranial x enografts harboring either prototypic FGFR4 (G388) or polymorphic FGFR4 (R388)

GH4C1 cells are known to coexpress GH and PRL. Furthermore, in the in vitro setting, GH4C1 cells transfected with prototypic FGFR4 (G388) have previously been shown to express increased levels of PRL relative to GH, whereas the opposite pattern is observed in the polymorphic variant (R388), with higher levels of GH relative to PRL (13). To investigate whether such a pattern is observed in our in vivo xenograft models, we examined the expression of these hormones in our intracranial tumor model using IHC analysis.

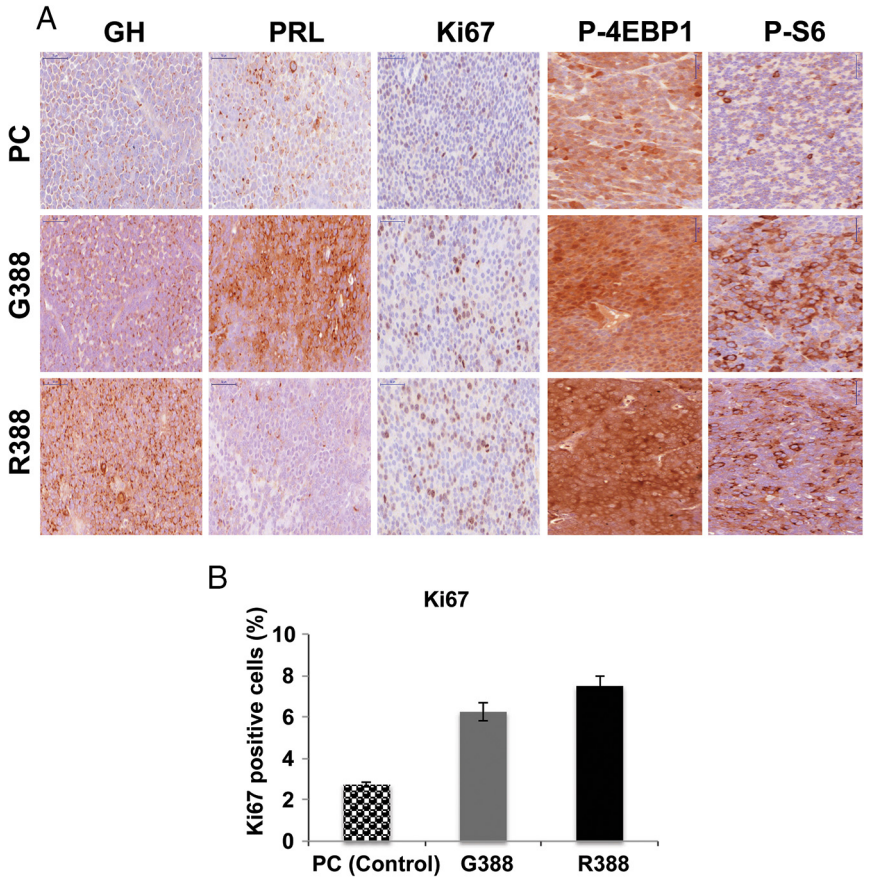

Figure 2. IHC stainings showing GH, PRL, Ki-67, p-4EBP1, and p-S6 protein expression levels in pituitary GH4C1 intracranial tumors (PC, G388, and R388). A, G388 produces a proliferating tumor with enhanced PRL production and diminished GH production, whereas injection of R388 cells produce a proliferating tumor with diminished PRL expression and enhanced GH expression (n = 5) (magnification, × 40; scale, 50 μm). IHC staining of p-S6 and p-4EBP1 in intracranial xenograft mouse GH4C1 tumors transfected with either G388 or R388 reveals widespread expression compared with PC tumors (n = 5) (magnification, × 40; scale bar, 50 μm). B, Bar graphs showing quantification of ki67 staining in PC, G388, and R388 tumors using ImageJ (National Institutes of Health, Bethesda, Maryland). Data show increased number of Ki-67-positive cells in G388 and R388 compared with PC tumors (n = 3, $P < .001$).

Our data show that G388 tumors have an increased expression of PRL compared with GH, whereas the R388 tumors have higher expression of GH compared with PRL (Figure 2A), confirming previous in vitro data.

Intracranial GH4C1 tumors transfected with either prototypic FGFR4 (G388) or polymorphic FGFR4 (R388) exhibit abundant mTOR signaling

Pituitary adenoma cells have been shown to express activated mTOR in vitro (16, 18). We investigated the activation status of the mTOR signaling pathway molecules in our GH4C1 tumors using the phosphorylation level of the immediate downstream effectors, S6 and 4EBP1, as a readout for mTOR activity. Our data show that there was abundant staining of both p-S6 and p-4EBP1 in all GH4C1 tumors examined, with G388 and R388 tumors showing increased p-S6 and p-4EBP1 compared with PC (Figure 2A), supporting that our model is appropriate for testing the effects of mTOR inhibition therapy.

Inhibition of mTOR signaling using RAD001 decreases intracranial GH4C1 tumor volume, regardless of FGFR4 status

In vitro analysis of pituitary adenoma cells has shown that these cells respond to mTOR inhibitors, including RAD001, with a reduction in cell proliferation and viability (18, 19). To assess the effects of RAD001 in our intracranial tumor model, we treated mice bearing PC, G388, and R388 with 5 mg/kg RAD001 or vehicle (n = 60) for 3 weeks, starting when tumors reached a predefined volume threshold of 1–5 mm^3 as assessed by MRI. Our data showed a significant reduction in tumor volume and growth rate in all three groups of the mice that were treated with RAD001 (Figure 3, A–C). The magnitude of the growth rate reduction was not statistically significant in all three different cell types (PC, G388, and R388) with RAD001 treatment: 2.1-, 2.2-, and 2.4-fold in PC, G388, and R388 tumors, respectively (Figure 3C).

Inhibition of mTOR by RAD001 decreases p-S6 level in intracranial GH4C1 tumors transfected with either prototypic FGFR4 (G388) or polymorphic FGFR4 (R388)

Activation of the mTOR pathway increases the p-S6 protein in various cancers, including PA (19, 25). It has been shown that in human and animal PA cells, inhibition of mTOR signaling results in reduced p-S6 levels. To investigate the effect of mTOR inhibition on the p-S6 level, we treated the mice harboring the PC control, G388, or R388 tumors with RAD001 and examined the expression of p-S6 using IHC and Western blot analysis. Both IHC and Western blot analysis data showed a significant reduction of the p-S6 level in all three groups of the mice treated with RAD001 (Figure 4, A–C). We also examined the phosphorylation of 4EBP1,

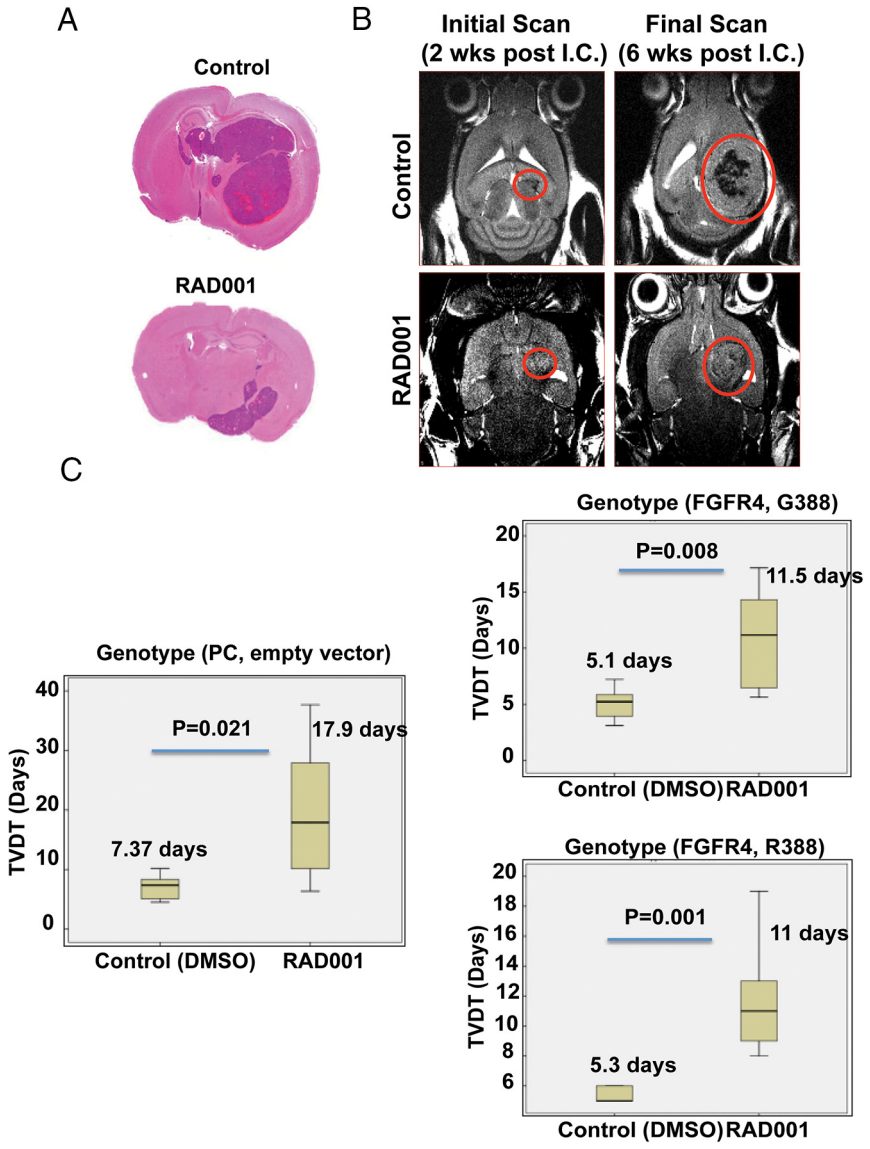

Figure 3. MRI and volumetric comparison of treated (RAD001) and untreated control groups. A, Intracranial GH4C1 tumor in control group exhibiting representative large, hemorrhagic tumors (top panel) as indicated on hematoxylin and eosin-stained, formalin-fixed, paraffin-embedded brain tissue sections. B, Axial T2-weighted MRI scans showing intracranial GH4C1 tumors treated with 5 mg/kg RAD001 were typically smaller than in control nontreated mice. C, The growth rates for 25 intracranial GH4C1 tumors (PC, G388, or R388) calculated as TVDT and displayed as box plot (n = 8 for each PC, G388, and R388 group). The median growth rates are reported. The growth rates in all three groups decreased after RAD001 treatment, although the magnitude of the decrease was similar in all groups. DMSO, dimethylsulfoxide. Abbreviation: I.C., intracranial.

an alternate immediate downstream effector of mTOR signaling, in all three groups of the mice. Contrary to what was seen with p-S6, the initial increase in p-4EBP1 was not attenuated after treatment with RAD001 (Figure 4D).

Inhibition of mTOR by RAD001 decreases GH expression and serum IGF-1 secretion in intracranial GH4C1 tumors transfected with either prototypic FGFR4 (G388) or polymorphic FGFR4 (R388)

GH expression and IGF-1 secretion in GH4C1 xenograft models have not been previously investigated with respect to mTOR inhibition. In our xenograft model, we investigated the effects of mTOR inhibition on the expression of GH and its systemic effector, IGF-1. Based on our data, there was an increased level of GH expression in the R388 tumors compared with either the G388 or PC control tumors, and this difference was statistically significant (Figure 5, A–C). Our data also showed a significant increase in IGF-1 secretion in the R388 tumors compared with either the G388 or PC control ($P < .05$) (Figure 5D). After treatment with RAD001, the R388 tumors displayed a significant reduction in both GH expression and serum IGF-1 secretion compared with the PC and G388 tumors, indicating that the R388 polymorphism can be used as a model to study the molecular mechanisms of GH expression to monitor the response to targeted therapies (Figure 5, A–D).

Discussion

Consistent molecular aberrations that underlie the formation and progression of sporadic PAs are not clearly defined. To identify and characterize the biological impact of a proposed pathophysiological mechanism involved in PAs, a robust in vivo model of PA is necessary. To date, a number of models of PA have been generated, but these have primarily harbored genetic mutations that do not mimic the human disease. For example, transgenic mice possessing a dopamine D2 receptor knockout or p27 deletion do develop PAs, but these are uncharacteristic of the human situation in that, in humans, these genes are not generally altered (26, 27). Furthermore, these PA models sometimes progress through a hyperplastic stage before becoming neoplastic (26, 28), which is not a common phenomenon that is seen clinically. In this study we have generated a reproducible intracranial xenograft model of PA that closely approximates the sporadic nature of the vast majority of PAs in that the mouse model we use does not harbor any genetic mutations.

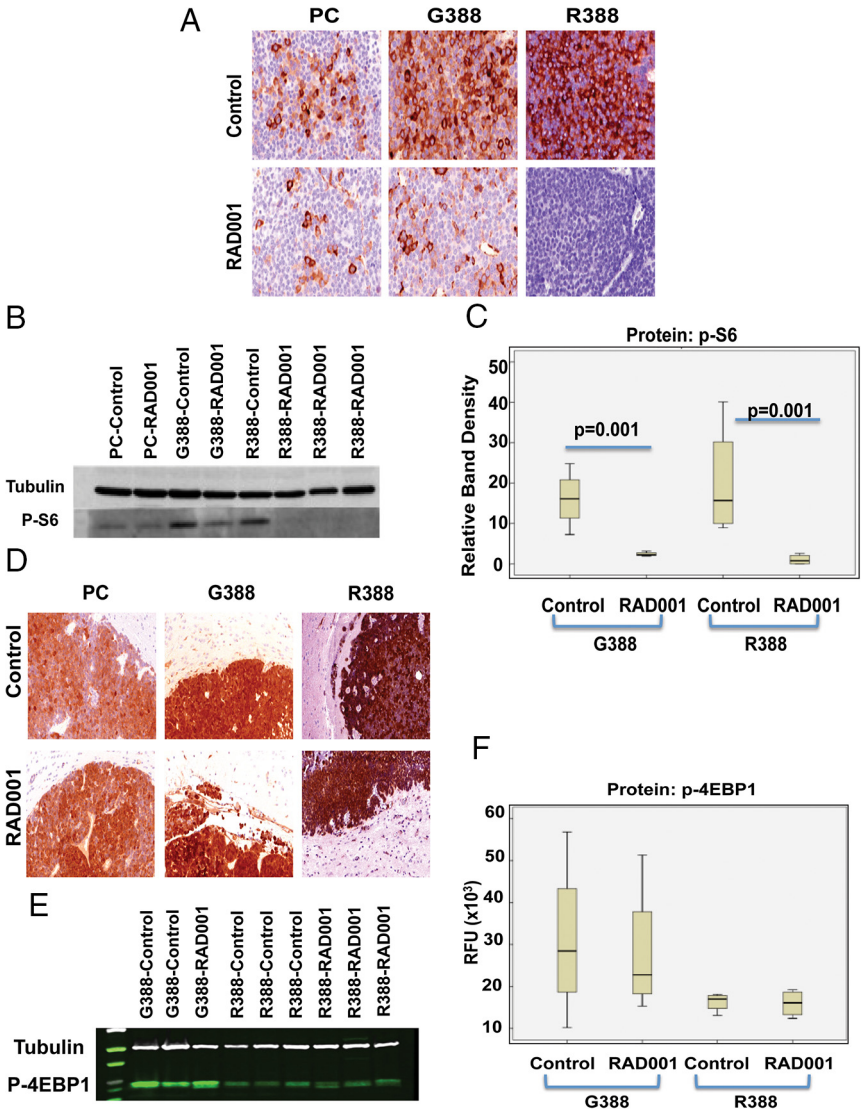

Figure 4. IHC staining of p-S6 and p-4EBP1 levels in three different GH4C1 cell groups (PC, G388, and R388) treated with RAD001 or vehicle. A, IHC staining of p-S6 in GH4C1 tumors transfected with PC, G388, or R388 shows a decrease after treatment with RAD001 (n = 5) (magnification, ×40; scale bar, 50 μm). B, Equal amounts of tumor lysates were resolved by SDS-PAGE and analyzed by immunoblotting with p-S6 (32 kDa) and tubulin (50 kDa). C, Quantification of protein was conducted using LI-COR software and the intensity of the p-S6 band was compared with intensity of the loading control (tubulin). Results are reported in relative fluorescence units (RFUs) and displayed in boxplot format. Median p-S6 band intensity was significantly attenuated in both G388 and R388 tumors after mTOR inhibition with RAD001 (n = 5). D, IHC analysis of p-4EBP1 expression in GH4C1 tumors transfected with PC, G388, or R388 shows no change in expression after treatment with RAD001 (n = 5) (magnification, ×20; scale bar, 50 μm). E, Equal amounts of tumor lysates were resolved by SDS-PAGE and analyzed by immunoblotting with p-4EBP1 (20 kDa) and tubulin (50 kDa). F, Quantification analysis show that median p-4EBP1 band intensity was not significantly altered in either G388 or R388 tumors after mTOR inhibition with RAD001 (n = 5).

The tumor growth rate, as assessed by TVDT, was examined in our cell lines as described previously (29, 30). Our preliminary experiments showed that the GH4C1 cells transfected with empty vector (PC), wild-type FGFR4-G388, and the FGFR4-R388 tumors developed in approximately 3 weeks. Validation of our initial experiments revealed that the PC tumors tended to grow the slowest (longest TVDT); however, the difference in growth rates between the untreated tumors of the PC, G388, and R388 tumors was not significant.

The mTOR pathway, which is frequently up-regulated in various cancers, has been shown to be a viable molecular marker for PA (16). Several papers have shown that various upstream and downstream components from mTOR, including mTOR itself, are up-regulated in animal and human PA tissue (16, 31, 32). The GH4C1 PA tumor models generated in this study demonstrate the expression of mTOR; in particular, there is an abundant phosphorylation levels of the two target proteins of mTOR, S6 and 4EBP1, which are the typical readouts for mTOR activation and are both critical for the positive regulation of protein synthesis. Both p-S6 and p-4EBP1 were higher in G388 and R388 tumors compared with PC tumors.

The mTOR inhibiting agent rapamycin and its analogs including RAD001 are potent immunosuppressants, which are also used for their antiproliferative properties. Rapamycin and RAD001 have been shown to be effective in various endocrine and nonendocrine cancers and have also demonstrated efficacious preclinical treatment effects in PA. Here we demonstrate that intracranial xenograft models, which harbor different FGFR4 genotypes, are equally susceptible to mTOR inhibition. There is currently one other study implicating mTOR signaling with respect to the FGFR4-G388R SNP in pancreatic neuroendocrine cells (33). In their study, it was revealed that the wild-type FGFR4-G388 tumors responded to RAD001, whereas the tumors harboring the SNP were resistant to mTOR inhibition. In our model, RAD001 treatment resulted in reduced tumor volume and growth rate (as assessed by a TVDT), but these reductions were of similar magnitude in all cell groups (~2 times the reduction in growth for pc, G388, and R388 tumors).

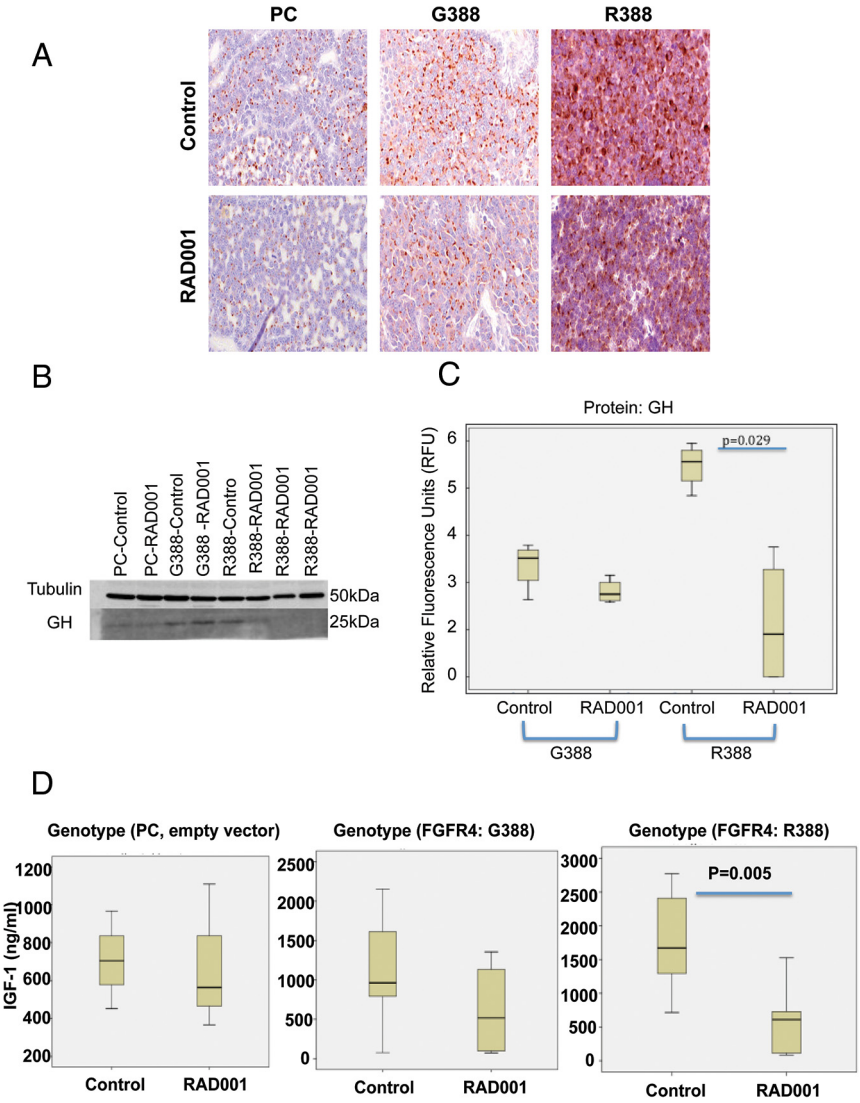

Figure 5. GH expression and IGF-1 secretion in three GH4C1 cell groups (PC, G388, andR388) treated with RAD001 or vehicle. A, IHC staining showing R388 tumors exhibit enhanced GH expression with decreased expression levels after treatment with RAD001 (n = 5) (magnification. ×40; scale, bar, 50 μm). B, Equal amounts of tumor lysates. Twenty-six were resolved by SDS-PAGE and analyzed by immunoblotting with GH (25 kDa) and tubulin (50 kDa). C, Quantification analysis showed that median GH protein band intensity was enhanced in R388 groups and demonstrated a significant reduction in GH protein levels after mTOR inhibition with RAD001 (n = 5). D, Circulating IGF-1 levels as a measure of GH4C1 tumor output are noted in PC, G388, and R388 groups. Median IGF-1 levels are enhanced in the R388 group and display a significant decrease in IGF-1 levels after mTOR inhibition with RAD001 (P = .005).

The difference in treatment response between the two studies may be attributed to the nature of cells. In the study by Serra et al (33), aggressive, metastatic neuroendocrine pancreatic cancer cell lines were used to establish their xenograft model.

We found that a reduced growth rate was associated with a decrease in the p-S6 level. The drug-induced reduction in the phosphorylation level of S6 could be due to a decrease in total S6 protein or as a result of reduced S6 phosphorylation. In either case, this study shows that RAD001 inhibits activation of S6. It has been demonstrated previously by other groups that, after mTOR inhibition, rapamycin resistance is promoted by the reduction of S6, leading to an elimination of the negative feedback loop to insulin receptor substrate-1, resulting in Akt activation. It has been reported that this phenomenon is not seen in the GH cell lines (18). This was also not seen in our GH4C1 tumors because we initially used octreotide, which abrogates Akt expression, in addition to RAD001, and the combination did not reveal any synergistic antiproliferative effects. Furthermore, Akt expression in our tumor model was weak, suggesting that mTOR activation may have occurred by other signaling mechanisms.

We found that the phosphorylation of the parallel downstream effector of mTOR, 4EBP1, is elevated, but this increase was not affected by RAD001 in our animals. There is evidence supporting this phenomenon in which long-term treatment promotes a rebound effect of p-4EBP1 and the reinitiation of protein translation (33). It has been demonstrated that p-4EBP1 may become rapamycin (or rapalog) insensitive over time. The treatment period we implemented lasted for a period of 3 weeks, which may have been long enough to promote rapamycin insensitivity. The rebound effect of p-4EBP1 restimulates mRNA translation and may provide a possible explanation for our GH4C1 tumors exhibiting a slower growth rate but not a complete cessation of growth or regression. Other studies have shown a reduced expression pattern of the mTOR pathway after mTOR inhibition, but correlating this attenuation with a quantified lower growth rate has not been performed previously.

The cells that we used to generate our model were transfected with FGFR4. Prototypic FGFR4 is a 110-kDa membrane protein consisting of three extracellular Ig-like domains, a transmembrane domain, a split tyrosine kinase cytoplasmic domain, and a Carboxyl tail. The FGFR4 used in our GH4C1 models was membrane bound and harbored a SNP in its transmembrane domain (discussed

below). Our GH4C1 tumors transfected with prototypic FGFR4 were quite aggressive but did respond to mTOR inhibition with reduced mTOR signaling and a lower growth rate. Previous work with human data demonstrates that FGFR4 was not associated with tumor size in patients harboring a somatotroph adenoma. However, in ACTH-PA, the FGFR4 allele was associated with small hormonally active ACTH-secreting microadenomas. Another study showed that a correlation exists between homozygous wild-type FGFR4 genotype and postoperative recurrence in patients with Cushing's disease (35). Thus, the wild-type FGFR4 may play a more integral role in the pathology of human ACTH tumors relative to GH-PA (15).

In addition to prototypic FGFR4, we also used an FGFR4 variant that harbored a germline SNP at codon 388, resulting in the presence of a glycine-to-arginine substitution in the transmembrane domain of the FGFR4 protein. At least one allele for this SNP is present in approximately half of the general population, indicating that this is a clinically relevant polymorphism. The literature regarding the role of this FGFR4-G388R SNP in cancer has largely been correlative and suggests that it is associated with poorer clinical outcome. Data regarding downstream mechanisms from the FGFR4-R388 SNP remain unclear. There are two studies to date implicating this SNP in ACTH-PA and GH-PA and suggests that src and serine STAT3 phosphorylation is responsible for cell prolifera-

Table 1. Antibody Table

Peptide/Protein Target	Antigen Sequence (if Known)	Name of Antibody	Manufacturer, Catalog Number, and/or Name of Individual Providing the Antibody	Species Raised (Monoclonal or Polyclonal)	Dilution Used
Rat pituitary growth hormone		GH	Antiserum created by Dr A. F. Parlow (Scientific Director, National Hormone and Pituitary Program, Harbor-UCLA Medical Center, Torrance, California; http://www.humc.edu/hormones/material.html	Rabbit	1:1 000 000
Rat pituitary PRL		Prolactin	Antiserum created by Dr A. F. Parlow, Scientific Director, National Hormone and Pituitary Program, Harbor-UCLA Medical Center, Torrance, California; http://www.humc.edu/hormones/material.html	Rabbit polyclonal	1:600 000
Human recombinant peptide corresponding to a 1002-bp Ki-67 cDNA fragment		Ki67	Dako	Mouse monoclonal	1:100
Phospho-S6 ribosomal protein (Ser240/244) (D68F8) XP rabbit mAb detects endogenous levels of ribosomal protein S6 only when phosphorylated at Ser240 and Ser244		p-S6	Cell signaling	Rabbit monoclonal	1:2000
Phospho-4EBP1 (Thr37/46) (236B4) rabbit mAb detects endogenous levels of 4EBP1 only when phosphorylated at Thr37 and/or Thr46		p-4EBP1	Cell signaling	Rabbit monoclonal	1:1000
Monoclonal antibody is produced by immunizing animals with a synthetic peptide corresponding to the amino terminus of human α-tubulin protein		Tubulin	Cell signaling	Rabbit monoclonal	1:1000

Abbreviation: mAb, monoclonal antibody.

tion, whereas tyrosine STAT3 phosphorylation modulates hormone secretion (13, 15). Clinically, the SNP allele is associated with increased tumor size and GH levels as well as the presence of large hormonally inactive corticotroph macroadenomas in humans.

In our GH4C1 tumors, GH expression and IGF-1 secretion were noted. Interestingly, after mTOR inhibition with RAD001, GH expression was reduced with a significant attenuation in IGF-1 levels seen only in the R388 mice. It may be that RAD001 disrupts a connection in which GH is unable to stimulate IGF-1 secretion, specifically in tumors with aberrant FGFR4. Recently it has been demonstrated that tyrosine phosphorylation of STAT3 may regulate GH levels (13), and it may be through this pathway that RAD001 exerts its hormone-attenuating effects. There is one study to date that has reported, at the in vitro level, that mTOR inhibition abrogates IGF-1-mediated effects in human PA cells (19). In summary, our characterization of the role of mTOR inhibitors warrants further investigation because it has important therapeutic implications for patients with PA and, more specifically, those with GH tumors, which harbor the FGFR4-R388 allele.

Appendix

Acknowledgments

We thank Dr. Shereen Ezzat, senior scientist from Princess Margaret Cancer Centre for his critical advice and guidance during the course of this study. We also thank Mrs Kelly Burrell, Dr. Zadeh lab manager, for organizing and facilitating laboratory needs in order to achieve research goals in a timely efficient manner. Due to administrative error both names were omitted from the final submission in error and we would like to ensure recognition of Dr Ezzat to the work through creation of the cell lines, supervision of EM and TT, in addition to invaluable guidance on the project.

Address all correspondence and requests for reprints to: Gelareh Zadeh, MD, PhD, FRCSC, Division of Neurosurgery, Toronto Western Hospital, 399 Bathurst Street, West Wing, Fourth Floor, Toronto, ON, Canada M5T 2S8. E-mail: gelareh.zadeh@uhn.ca.

This work was supported by the Canadian Institute of Health Research.

Disclosure Summary: The authors have nothing to disclose.

References

1. **Asa SL, Ezzat S.** Molecular basis of pituitary development and cytogenesis. *Front Horm Res*. 2004;32:1–19.
2. **Mete O, Asa SL.** Clinicopathological correlations in pituitary adenomas. *Brain Pathol*. 2012;22(4):443–453.
3. **Knosp E, Steiner E, Kitz K, Matula C.** Pituitary adenomas with invasion of the cavernous sinus space: a magnetic resonance imaging classification compared with surgical findings. *Neurosurgery*. 1993; 33(4):610–617; discussion 617–618.
4. **Monsalves E, Larjani S, Loyola Godoy B, et al.** Growth patterns of pituitary adenomas and histopathological correlates. *J Clin Endocrinol Metab*. 2014;99(4):1330–1338.
5. **Vallar L, Spada A, Giannattasio G.** Altered Gs and adenylate cyclase activity in human GH-secreting pituitary adenomas. *Nature*. 1987; 330(6148):566–568.
6. **Pei L, Melmed S, Scheithauer B, Kovacs K, Prager D.** H-ras mutations in human pituitary carcinoma metastases. *J Clin Endocrinol Metab*. 1994;78(4):842–846.
7. **Ezzat S, Zheng L, Smyth HS, Asa SL.** The c-erbB-2/neu proto-oncogene in human pituitary tumours. *Clin Endocrinol (Oxf)*. 1997; 46(5):599–606.
8. **Ezzat S, Smyth HS, Ramyar L, Asa SL.** Heterogenous in vivo and in vitro expression of basic fibroblast growth factor by human pituitary adenomas. *J Clin Endocrinol Metab*. 1995;80(3):878–884.
9. **Abbass SA, Asa SL, Ezzat S.** Altered expression of fibroblast growth factor receptors in human pituitary adenomas. *J Clin Endocrinol Metab*. 1997;82(4):1160–1166.
10. **Asa SL, Ezzat S.** The pathogenesis of pituitary tumours. *Nat Rev Cancer*. 2002;2(11):836–849.
11. **Ezzat S, Zheng L, Asa SL.** Pituitary tumor-derived fibroblast growth factor receptor 4 isoform disrupts neural cell-adhesion molecule/N-cadherin signaling to diminish cell adhesiveness: a mechanism underlying pituitary neoplasia. *Mol Endocrinol*. 2004;18(10):2543–2552.
12. **Bange J, Prechtl D, Cheburkin Y, et al.** Cancer progression and tumor cell motility are associated with the FGFR4 Arg(388) allele. *Cancer Res*. 2002;62(3):840–847.
13. **Tateno T, Asa SL, Zheng L, Mayr T, Ullrich A, Ezzat S.** The FGFR4–G388R polymorphism promotes mitochondrial STAT3 serine phosphorylation to facilitate pituitary growth hormone cell tumorigenesis. *PLoS Genet*. 2011;7(12):e1002400.
14. **Ezzat S, Zheng L, Winer D, Asa SL.** Targeting N-cadherin through fibroblast growth factor receptor-4: distinct pathogenetic and therapeutic implications. *Mol Endocrinol*. 2006;20(11):2965–2975.
15. **Nakano-Tateno T, Tateno T, Hlaing MM, et al.** FGFR4 polymorphic variants modulate phenotypic features of Cushing disease. *Mol Endocrinol*. 2014;28(4):525–533.
16. **Musat M, Korbonits M, Kola B, et al.** Enhanced protein kinase B/Akt signalling in pituitary tumours. *Endocr Relat Cancer*. 2005; 12(2):423–433.
17. **Sajjad EA, Zielinski G, Maksymowicz M, Hutnik L, Bednarczuk T, Wlodarski P.** mTOR is frequently active in GH-secreting pituitary adenomas without influencing their morphopathological features. *Endocr Pathol*. 2013;24(1):11–19.
18. **Gorshtein A, Rubinfeld H, Kendler E, et al.** Mammalian target of rapamycin inhibitors rapamycin and RAD001 (everolimus) induce anti-proliferative effects in GH-secreting pituitary tumor cells in vitro. *Endocr Relat Cancer*. 2009;16(3):1017–1027.
19. **Zatelli MC, Minoia M, Filieri C, et al.** Effect of everolimus on cell viability in nonfunctioning pituitary adenomas. *J Clin Endocrinol Metab*. 2010;95(2):968–976.
20. **Burrell K, Hill RP, Zadeh G.** High-resolution in-vivo analysis of normal brain response to cranial irradiation. *PloS One*. 2012;7(6): e38366.
21. **Jalali S, Chung C, Foltz W, et al.** MRI biomarkers identify the differential response of glioblastoma multiforme to anti-angiogenic therapy. *Neuro Oncol*. 2014;16(6):868–879.
22. **Yushkevich PA, Piven J, Hazlett HC, et al.** User-guided 3D active contour segmentation of anatomical structures: significantly im-

proved efficiency and reliability. *NeuroImage*. 2006;31(3):1116–1128.
23. **Nakaguchi H, Fujimaki T, Matsuno A, et al.** Postoperative residual tumor growth of meningioma can be predicted by MIB-1 immunohistochemistry. *Cancer*. 1999;85(10):2249–2254.
24. **Ebinu JO, Lwu S, Monsalves E, et al.** γ Knife radiosurgery for the treatment of cystic cerebral metastases. *Int J Radiat Oncol Biol Physics*. 2013;85(3):667–671.
25. **Advani SH.** Targeting mTOR pathway: a new concept in cancer therapy. *Ind J Med Paediatr Oncol*. 2010;31(4):132–136.
26. **Friedman E, Adams EF, Hoog A, et al.** Normal structural dopamine type 2 receptor gene in prolactin-secreting and other pituitary tumors. *J Clin Endocrinol Metab*. 1994;78(3):568–574.
27. **Ikeda H, Yoshimoto T, Shida N.** Molecular analysis of p21 and p27 genes in human pituitary adenomas. *Br J Cancer*. 1997;76(9):1119–1123.
28. **Asa SL, Kelly MA, Grandy DK, Low MJ.** Pituitary lactotroph adenomas develop after prolonged lactotroph hyperplasia in dopamine D2 receptor-deficient mice. *Endocrinology*. 1999;140(11):5348–5355.
29. **Hsu CY, Guo WY, Chien CP, Ho DM.** MIB-1 labeling index correlated with magnetic resonance imaging detected tumor volume doubling time in pituitary adenoma. *Eur J Endocrinol*. 2010;162(6):1027–1033.
30. **Tanaka Y, Hongo K, Tada T, Sakai K, Kakizawa Y, Kobayashi S.** Growth pattern and rate in residual nonfunctioning pituitary adenomas: correlations among tumor volume doubling time, patient age, and MIB-1 index. *J Neurosurg*. 2003;98(2):359–365.
31. **Kenerson H, Dundon TA, Yeung RS.** Effects of rapamycin in the Eker rat model of tuberous sclerosis complex. *Pediatr Res*. 2005;57(1):67–75.
32. **Lu C, Willingham MC, Furuya F, Cheng SY.** Activation of phosphatidylinositol 3-kinase signaling promotes aberrant pituitary growth in a mouse model of thyroid-stimulating hormone-secreting pituitary tumors. *Endocrinology*. 2008;149(7):3339–3345.
33. **Serra S, Zheng L, Hassan M, et al.** The FGFR4–G388R single-nucleotide polymorphism alters pancreatic neuroendocrine tumor progression and response to mTOR inhibition therapy. *Cancer Res*. 2012;72(22):5683–5691.